

AD-A200 327

THE DISK: A COMPARISON OF ELECTROMAGNETIC SCATTERING
SOLUTIONS AND ITS USE (U) HOME AIR DEVELOPMENT CENTER
GRIFFISS AFB NY K D TROTT FEB 88 RADC-YR-88-16

1/1

UNCLASSIFIED

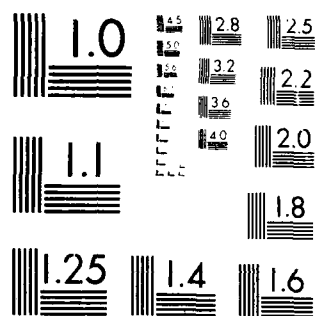
F/G 17/9

ML

END

DATE

1-88



DTIC FILE COPY

2

AD-A200 327

RADC-TR-88-16

**In-House Report
February 1988**



**THE DISK: A COMPARISON OF
ELECTROMAGNETIC SCATTERING
SOLUTIONS AND ITS USE AS A
CALIBRATION STANDARD FOR BISTATIC
RCS MEASUREMENTS**

Keith D. Trott, Capt, USAF

DTIC
ELECTE
NOV 04 1988
S D
CH

APPROVED FOR PUBLIC RELEASE; DISTRIBUTION UNLIMITED

**ROME AIR DEVELOPMENT CENTER
Air Force Systems Command
Griffiss Air Force Base, NY 13441-5700**

88 11 4 012

This report has been reviewed by the RADC Public Affairs Office (PA) and is releasable to the National Technical Information Service (NTIS). At NTIS it will be releasable to the general public, including foreign nations.

RADC-TR-88-16 has been reviewed and is approved for publication.

APPROVED:



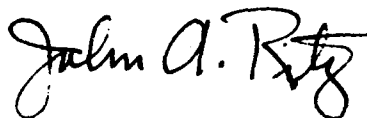
J. LEON POIRIER
Chief, Applied Electromagnetics Division
Directorate of Electromagnetics

APPROVED:



JOHN K. SCHINDLER
Acting Director
Directorate of Electromagnetics

FOR THE COMMANDER:



JOHN A. RITZ
Directorate of Plans & Programs

If your address has changed or if you wish to be removed from the RADC mailing list, or if the addressee is no longer employed by your organization, please notify RADC (EECT) Hanscom AFB MA 01731-5000. This will assist us in maintaining a current mailing list.

Do not return copies of this report unless contractual obligations or notice on a specific document requires that it be returned.

Unclassified

SECURITY CLASSIFICATION OF THIS PAGE

REPORT DOCUMENTATION PAGE				Form Approved OMB No. 0704-0188		
1a. REPORT SECURITY CLASSIFICATION Unclassified			1b. RESTRICTIVE MARKINGS N/A			
2a. SECURITY CLASSIFICATION AUTHORITY N/A			3. DISTRIBUTION/AVAILABILITY OF REPORT Approved for public release; distribution unlimited.			
2b. DECLASSIFICATION/DOWNGRADING SCHEDULE N/A						
4. PERFORMING ORGANIZATION REPORT NUMBER(S) RADC-TR-88-16			5. MONITORING ORGANIZATION REPORT NUMBER(S)			
6a. NAME OF PERFORMING ORGANIZATION Rome Air Development Center		6b. OFFICE SYMBOL (if applicable) EECT	7a. NAME OF MONITORING ORGANIZATION Rome Air Development Center (EECT)			
6c. ADDRESS (City, State, and ZIP Code) Hanscom AFB Massachusetts 01731-5000			7b. ADDRESS (City, State, and ZIP Code) Hanscom AFB Massachusetts 01731-5000			
8a. NAME OF FUNDING/SPONSORING ORGANIZATION Rome Air Development Center		8b. OFFICE SYMBOL (if applicable) EECT	9. PROCUREMENT INSTRUMENT IDENTIFICATION NUMBER N/A			
8c. ADDRESS (City, State, and ZIP Code) Hanscom AFB Massachusetts 01731-5000			10. SOURCE OF FUNDING NUMBERS			
			PROGRAM ELEMENT NO 61102F	PROJECT NO 2305	TASK NO J4	WORK UNIT ACCESSION NO 04
11. TITLE (Include Security Classification) The Disk: A Comparison of Electromagnetic Scattering Solutions and Its Use as a Calibration Standard for Bistatic RCS Measurements						
12. PERSONAL AUTHOR(S) Keith D. Trott, Capt, USAF						
13a. TYPE OF REPORT In-House		13b. TIME COVERED FROM Sep 86 to Sep 87		14. DATE OF REPORT (Year, Month, Day) 1988 February		
15. PAGE COUNT						
16. SUPPLEMENTARY NOTATION N/A						
17. COSATI CODES			18. SUBJECT TERMS (Continue on reverse if necessary and identify by block number)			
FIELD	GROUP	SUB-GROUP	Scattering Calibration Disk			
09	03					
09	06					
19. ABSTRACT (Continue on reverse if necessary and identify by block number) <p>This report compares three solutions for scattering from a perfectly conducting disk. It compares a closed form Physical Optics (PO) solution, a solution found by applying the RADC/BSRCRCS scattering prediction code, and an exact eigenfunction solution. The results are compared for various ka values and incidence angles for both horizontal and vertical polarizations. In addition, this report determined the applicability of the disk as a calibration standard for bistatic radar cross section (RCS) measurements by examining the calibration curve. This curve is a plot of the specular return as a function of bistatic angle. This curve is computed for both horizontal and vertical polarizations at various ka values using the PO and eigenfunction solutions. Results show that PO agrees reasonably well with the PTD and eigenfunction solutions in certain cases. The agreement is particularly good for the calibration curve for a wide range of bistatic angles.</p>						
20. DISTRIBUTION/AVAILABILITY OF ABSTRACT <input checked="" type="checkbox"/> UNCLASSIFIED/UNLIMITED <input type="checkbox"/> SAME AS RPT <input type="checkbox"/> DTIC USERS			21. ABSTRACT SECURITY CLASSIFICATION Unclassified			
22a. NAME OF RESPONSIBLE INDIVIDUAL Keith D. Trott			22b. TELEPHONE (Include Area Code) (617) 377-4239		22c. OFFICE SYMBOL RADC/EECT	

DD Form 1473, JUN 86

Previous editions are obsolete.

SECURITY CLASSIFICATION OF THIS PAGE
Unclassified

Contents

1. INTRODUCTION	1
2. BISTATIC PHYSICAL OPTICS SOLUTION	3
3. RESULTS	9
4. CONCLUSIONS	13
REFERENCES	21

Illustrations

1. Disk Geometry	4
2. Incident Plane Geometry for Horizontal Pol (Pol = 90)	5
3. Incident Plane Geometry for Vertical Pol (Pol = 0)	6
4. Grazing Incidence ka Plot	10
5. Bistatic Scattering: $ka = 5$; Theta Inc = 0; Horiz Pol: Phi Inc = Phi Scat = 0	11
6. Bistatic Scattering: $ka = 5$; Theta Inc = 0; Vert Pol: Phi Inc = Phi Scat = 0	11
7. Bistatic Scattering: $ka = 10$; Theta Inc = 0; Horiz Pol: Phi Inc = Phi Scat = 0	12
8. Bistatic Scattering: $ka = 10$; Theta Inc = 0; Vert Pol: Phi Inc = Phi Scat = 0	12

Illustrations

9.	Bistatic Scattering: $k_a = 10$: Theta Inc = 15: Horiz Pol: Phi Inc = 0: Phi Scat = 180	14
10.	Bistatic Scattering: $k_a = 10$: Theta Inc = 15: Vert Pol: Phi Inc = 0: Phi Scat = 180	14
11.	Bistatic Scattering: $k_a = 10$: Theta Inc = 45: Horiz Pol: Phi Inc = 0: Phi Scat = 180	15
12.	Bistatic Scattering: $k_a = 10$: Theta Inc = 45: Vert Pol: Phi Inc = 0: Phi Scat = 180	15
13.	Bistatic Scattering: $k_a = 10$: Theta Inc = 70: Horiz Pol: Phi Inc = 0: Phi Scat = 180	16
14.	Bistatic Scattering: $k_a = 10$: Theta Inc = 70: Vert Pol: Phi Inc = 0: Phi Scat = 180	16
15.	Specular Scattering: $k_a = 5$: Horiz Pol	17
16.	Specular Scattering: $k_a = 5$: Vert Pol	17
17.	Specular Scattering: $k_a = 10$: Horiz Pol	18
18.	Specular Scattering: $k_a = 10$: Vert Pol	18
19.	Specular Scattering: $k_a = 20$: Horiz Pol	19
20.	Specular Scattering: $k_a = 20$: Vert Pol	19



Accession For	
NTIS GRA&I	<input checked="" type="checkbox"/>
DTIC TAB	<input type="checkbox"/>
Unannounced	<input type="checkbox"/>
Justification	
By	
Distribution/	
Availability Codes	
Dist	Avail and/or Special
A-1	

The Disk: A Comparison of Electromagnetic Scattering Solutions and Its Use as a Calibration Standard for Bistatic RCS Measurements

1. INTRODUCTION

This report compares three circular disk solutions: a closed form physical optics (PO) solution, the RADC/Syracuse Research Corp. bistatic radar cross-section (BSRCRCS) computer program that utilizes the physical theory of diffraction (PTD), and an exact eigenfunction solution discussed in References 2 through 4. These are compared for various ka values as well as incidence angles. The limitations of the PO solution are also discussed. As a by-product of this comparison, the BSRCRCS scattering code solution for the disk is validated against an exact eigenfunction solution. Another issue addressed in this report is the disk curve

(Received for publication 2 February 1988)

1. Bowman, J. J., Senior, T. B. A., and Uslenghi, P. L. E. (Eds.) (1969) Electromagnetic and Acoustic Scattering by Simple Shapes, Chapters 13 and 14; North Holland Pub. Co., Amsterdam.
2. Flammer, C. (1953) The vector wave function solution of the diffraction of electromagnetic waves by circular disks and apertures, I. Oblate spheroidal vector wave functions, II. The diffraction problem, J. Appl. Phys., 24(No. 9):1218-1231.
3. Mattson, G. R. (1970) Electromagnetic Plane Wave Scattering by a Perfectly Conducting Disk, Ph.D. Dissertation, University of Michigan.
4. Mithouard, D. P., and Hodge, D. B. (1979) Scattering by Metallic Disk, Report 710816-3, The Ohio State University Electroscience Laboratory, Dept. of Electrical Engineering.

used to calibrate a bistatic RCS measurement range. The disk calibration curve is a plot of the specular return as a function of bistatic angle. This curve will be computed for both horizontal and vertical polarizations and various ka values using the PO and eigenfunction solutions. The disk has become a possible calibration geometry for bistatic RCS measurement ranges due to problems encountered using the sphere. The bistatic RCS of a sphere has rapid fluctuations that make it difficult to use as a calibration standard for bistatic radar cross-section measurements.

The derivation of the PO solution is given in Section 2. The PO solution calculates the scattered field using the geometrical optics (GO) current, where the GO current is denoted by Ufimtsev⁵ as the uniform current. He also calculates the field scattered due to the non-uniform current on the edge of the disk. The superposition of fields scattered due to the uniform and non-uniform currents yields the total scattered field. This method is called the PTD. The BSRCRCS scattering code used in our comparison utilizes PTD as its method of solution; however, it is not a closed form solution. The BSRCRCS code is designed for arbitrarily shaped bodies and uses numerical techniques to perform the integrations required to implement the PTD method.

The disk is a coordinate surface in the oblate spheroidal coordinate system;¹ therefore, the exact eigenfunction solution can be found using the degenerate case of the oblate spheroidal functions when they collapse to a disk. Detailed discussions of this approach can be found in References 1, 2, 3, and 4. Mithouard and Hodge⁴ provide a computer program and subroutines required to calculate the RCS based on the eigenfunction solution. This computer program was modified by Dominek⁶ to allow its use for higher ka values. The program, as modified by Dominek, is used in this analysis. In addition, for grazing incidence of the horizontal polarization, this computer program was run as a function of ka to determine when the eigenfunction solution is no longer accurate. This was done to provide an upper bound on our use of the eigenfunction solution.

The details of the PTD and eigenfunction derivations are not discussed any further in this report. The references provided give detailed analyses of these methods. In the next section, we derive the PO based expression for the bistatic scattered field of a disk illuminated by a plane wave.

5. Ufimtsev, P. Ia. (1958) Approximate calculation of the diffraction of a plane electromagnetic wave by certain metal objects, II. The diffraction by a disk and by a finite cylinder, Soviet Physics - Technical Physics, 3(No. 11):2386-2396.

6. Dominek, A.K. personal communication.

2. BISTATIC PHYSICAL OPTICS SOLUTION

A version of this result is given without details in Reference 1, and the details can be found in Reference 5. The following result was derived independently because the results of References 2 and 5 have different assumptions, applicable geometry, and so on, than the eigenfunction and scattering code solutions; therefore, it was decided to rederive the result rather than to make the requisite modifications to the previous results.

The plane of incidence chosen is the xz plane ($\phi^i = 0$). The geometry for the disk is shown in Figure 1, and the geometry for horizontal and vertical polarizations are shown in Figure 2 and Figure 3. For our given plane of incidence, the incident \vec{E} and \vec{H} fields are given by

$$\vec{E}^i = \begin{pmatrix} \hat{\theta}^i \\ \hat{\phi}^i \end{pmatrix} e^{-j\vec{k}^i \cdot \vec{r}} \quad (1a)$$

$$\vec{H}^i = Y_0 \hat{r}^i \times \vec{E}^i \quad (1b)$$

where

$$Y_0 = 1/Z_0 = \sqrt{\epsilon/\mu} \quad , \quad (2a)$$

$$k = 2\pi/\lambda \quad , \quad (2b)$$

$$\vec{k}^i = k \hat{r}^i = -k (\hat{x} \sin \xi + \hat{z} \cos \xi) \quad , \quad (2c)$$

$$\hat{r}^i = -\hat{x} \sin \xi - \hat{z} \cos \xi \quad , \quad (2d)$$

$$\hat{\theta}^i = \hat{x} \cos \xi - \hat{z} \sin \xi \quad , \quad (2e)$$

$$\hat{\phi}^i = \hat{y} \quad , \quad (2f)$$

and

$$\vec{r} = x \hat{x} + y \hat{y} + z \hat{z} \quad . \quad (2g)$$

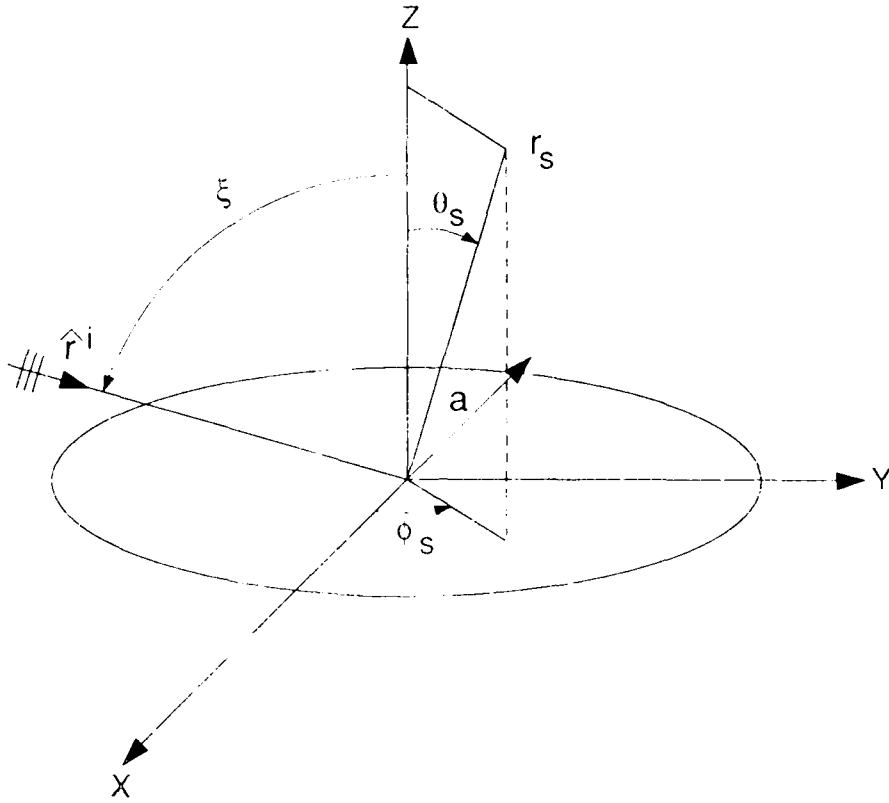


Figure 1. Disk Geometry

The upper and lower terms in Eq. (1a) and Eq. (1b) are for parallel (vertical or theta) and perpendicular (horizontal or phi) polarizations respectively. The polarization of the incident field is parallel/perpendicular with respect to our plane of incidence. In general, the GO current is given by

$$\bar{J}_{go} = 2 \hat{z} \times \bar{H}^i \Big|_{z'=0} ; \quad (3)$$

hence,

$$\bar{J}_{go} = 2 Y_o \begin{pmatrix} \hat{x} \\ \hat{y} \cos \xi \end{pmatrix} e^{jk\rho' \cos \phi' \sin \xi} . \quad (4)$$

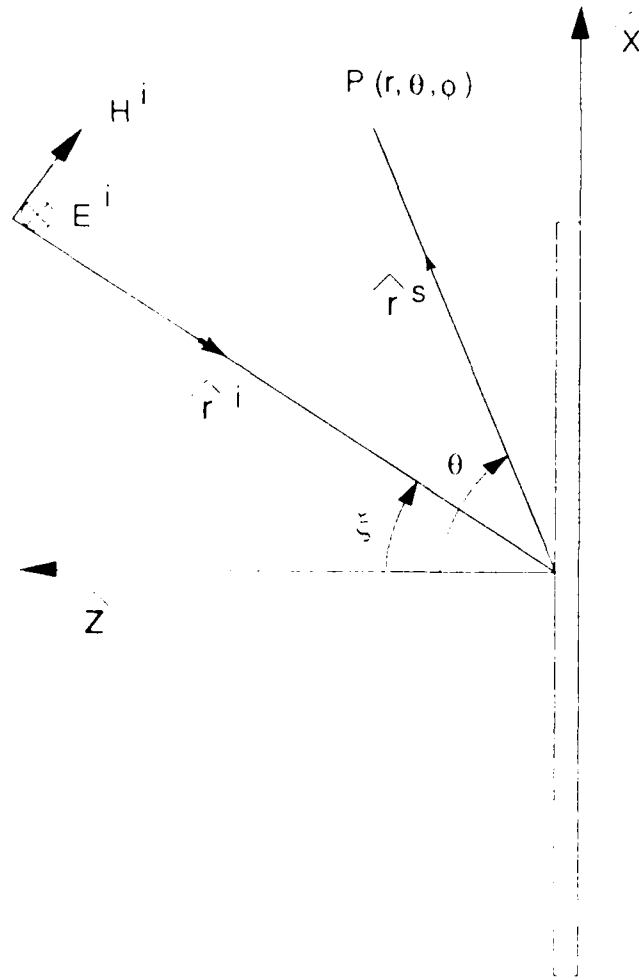


Figure 2. Incident Plane Geometry for Horizontal Pol (Pol = 90) || Edge

Using this current (making the usual far field approximations) yields an expression for the scattered field given by

$$\bar{E}_{po}^s = jk \frac{e^{-jk r}}{r} \left\{ \begin{array}{l} \hat{r} \times \hat{r} \times \hat{x} \\ \hat{r} \times \hat{r} \times \hat{y} \cos \xi \end{array} \right\} D(\theta, \phi, \xi) \quad (5)$$

where

$$D(\theta, \phi, \xi) = \frac{1}{2\pi} \int_0^a \rho' \int_0^{2\pi} e^{jk\rho'} [\sin \theta \cos(\phi - \phi') + \sin \xi \cos \phi'] d\phi' d\rho' . \quad (6)$$

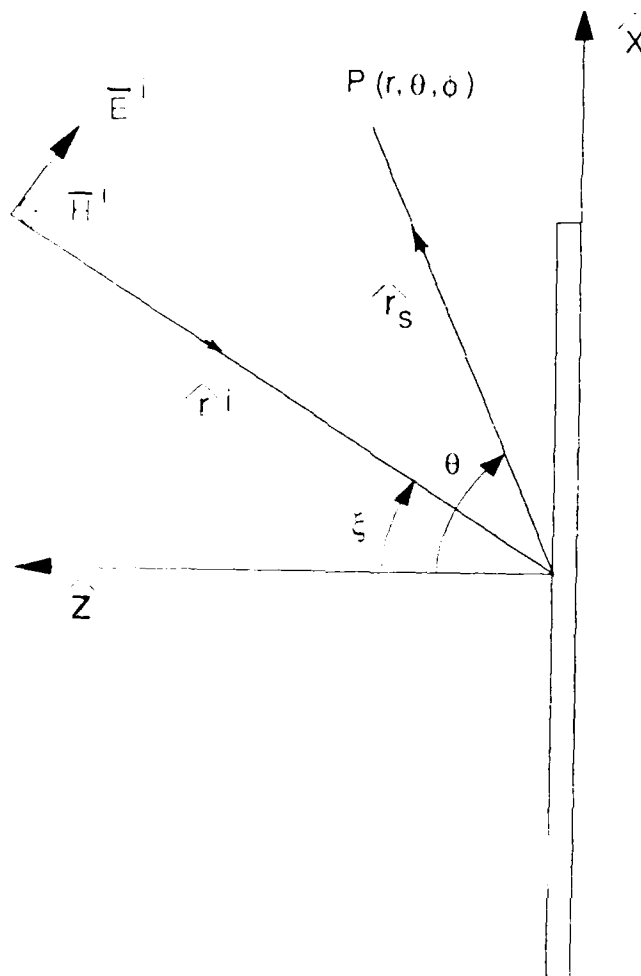


Figure 3. Incident Plane Geometry for Vertical Pol (Pol = 0) Edge

We can then write the phase term of the integrand in the form

$$\sin \theta \cos (\varphi - \varphi') + \sin \xi \cos \varphi' = \Omega \cos (\gamma - \varphi') \quad (7)$$

such that

$$\Omega \cos \gamma = \sin \xi + \sin \theta \cos \varphi, \quad (8a)$$

$$\Omega \sin \gamma = \sin \theta \sin \varphi, \quad (8b)$$

$$\Omega = \sqrt{\sin^2 \theta \sin^2 \varphi + (\sin \xi + \sin \theta \cos \varphi)^2}. \quad (8c)$$

Therefore, we write

$$D(\theta, \phi, \xi) = \int_0^a \rho' \frac{1}{2\pi} \int_0^{2\pi} e^{jk\rho' \Omega \cos(\gamma - \phi')} d\phi' d\rho' ; \quad (9)$$

however

$$\frac{1}{2\pi} \int_0^{2\pi} e^{jk\rho' \Omega \cos(\gamma - \phi')} d\phi' = J_0(k\Omega\rho') \quad (10)$$

where J_0 is the Bessel function of order zero. In addition,

$$\int_0^a \rho' J_0(k\Omega\rho') d\rho' = a \frac{J_1(ka\Omega)}{k\Omega} . \quad (11)$$

Hence, the PO scattered field is given by

$$\bar{E}_{po}^s = ja \frac{e^{-jkr}}{r} \frac{J_1(ka\Omega)}{\Omega} \begin{pmatrix} -\hat{\theta} \cos \theta \cos \phi + \hat{\phi} \sin \phi \\ -\cos \xi (\hat{\theta} \cos \theta \sin \phi + \hat{\phi} \cos \phi) \end{pmatrix} . \quad (12)$$

We want to identify specific input/output polarization pairs; that is, what is the theta polarized scattered field for a phi polarized incident field. We write this as $E_{\theta\phi}^s$. Therefore, we have the following:

$$E_{\theta\theta}^s = -ja \frac{e^{-jkr}}{r} \frac{J_1(ka\Omega)}{\Omega} \cos \theta \cos \phi , \quad (13a)$$

$$E_{\phi\theta}^s = ja \frac{e^{-jkr}}{r} \frac{J_1(ka\Omega)}{\Omega} \sin \phi , \quad (13b)$$

$$E_{\theta\phi}^s = -ja \frac{e^{-jkr}}{r} \frac{J_1(ka\Omega)}{\Omega} \cos \xi \cos \theta \sin \phi , \quad (13c)$$

$$E_{\phi\phi}^s = -ja \frac{e^{-jkr}}{r} \frac{J_1(ka\Omega)}{\Omega} \cos \xi \cos \phi . \quad (13d)$$

These expressions can be modified to match those given by Ufimtsev⁵ for the uniform current.

In general, the scattering cross section is defined by

$$\sigma = \lim_{r \rightarrow \infty} 4\pi r^2 \frac{|\vec{E}^s|^2}{|\vec{E}^i|^2} . \quad (14)$$

In addition, if we desire the polarization dependent cross section, we define

$$\sigma_{ab} = \lim_{r \rightarrow \infty} 4\pi r^2 \frac{|E_a^s|^2}{|E_b^i|^2} \quad (15)$$

where a and b represent either the theta or phi polarizations. Therefore, the input/output polarization dependent cross section based on Eqs. (13a) to (13d) is given by

$$\sigma_{\theta\theta} = 4\pi a^2 \left[\frac{J_1(ka\Omega)}{\Omega} \right]^2 \cos^2 \theta \cos^2 \phi , \quad (16a)$$

$$\sigma_{\phi\phi} = 4\pi a^2 \left[\frac{J_1(ka\Omega)}{\Omega} \right]^2 \sin^2 \phi , \quad (16b)$$

$$\sigma_{\theta\phi} = 4\pi a^2 \left[\frac{J_1(ka\Omega)}{\Omega} \right]^2 \cos^2 \xi \cos^2 \theta \sin^2 \phi , \quad (16c)$$

$$\sigma_{\phi\theta} = 4\pi a^2 \left[\frac{J_1(ka\Omega)}{\Omega} \right]^2 \cos^2 \xi \cos^2 \phi . \quad (16d)$$

It should be noted that when the argument of the Bessel function goes to zero we have

$$\lim_{\Omega \rightarrow 0} \frac{J_1(ka\Omega)}{\Omega} = \frac{ka}{2} J_0(0) = \frac{ka}{2} . \quad (17)$$

There are some special cases worth mentioning. In the case of backscatter,

$$\sigma = \pi a^2 J_1^2(2ka \sin \theta) \cot^2 \theta , \quad (18)$$

and for the specular case,

$$\sigma = \frac{4\pi}{\lambda^2} (\pi a^2 \cos \theta)^2 . \quad (19)$$

This has the proper form for specular scattering given by

$$\sigma_{\text{spec}} = \frac{4\pi}{\lambda^2} A^2 \quad (20)$$

where A is the projected area of the scatterer. Note, both the backscatter and specular expressions are independent of polarization.

These expressions were programmed and used for comparison with both the BSRCRCS scattering code and the eigenfunction code. The plots in Section 3 show where the bistatic PO solution for the disk breaks down. In addition, comparisons for the specular response using the PO and eigenfunction solutions will be shown. For our plane of incidence (xz plane), horizontal polarization has a component parallel to the edge; therefore, for edge-on incidence (incidence angle nearly 90°), the scattered field is not zero. The vertical polarization for edge-on incidence does not have a component parallel to the edge and hence the scattered field is zero. The eigenfunction satisfies the proper edge condition; therefore, we expect the proper behavior at the edge. This will be evident in our plots.

3. RESULTS

In this section, plots that compare the three solutions previously described are shown. In addition, calibration curves computed using the PO and eigenfunction solutions are also shown. However, before beginning the comparisons it is of interest to determine when the eigenfunction solution breaks down as a function of the electrical circumference of the disk (ka). For horizontal polarization, we plotted backscatter and forward scatter for grazing incidence. As expected, the backscatter case accounts for the creeping wave around the disk edge; hence, we see the interference lobes. On the other hand, the forward scatter is not affected by this mechanism and is therefore a smoother curve. Figure 4 shows this behavior. Also, we can see that the solution breaks down beyond $ka = 22$. Therefore, we only used this solution up to $ka = 20$.

SCATTERING FROM A DISK (GRAZING INC: HORIZ POL)

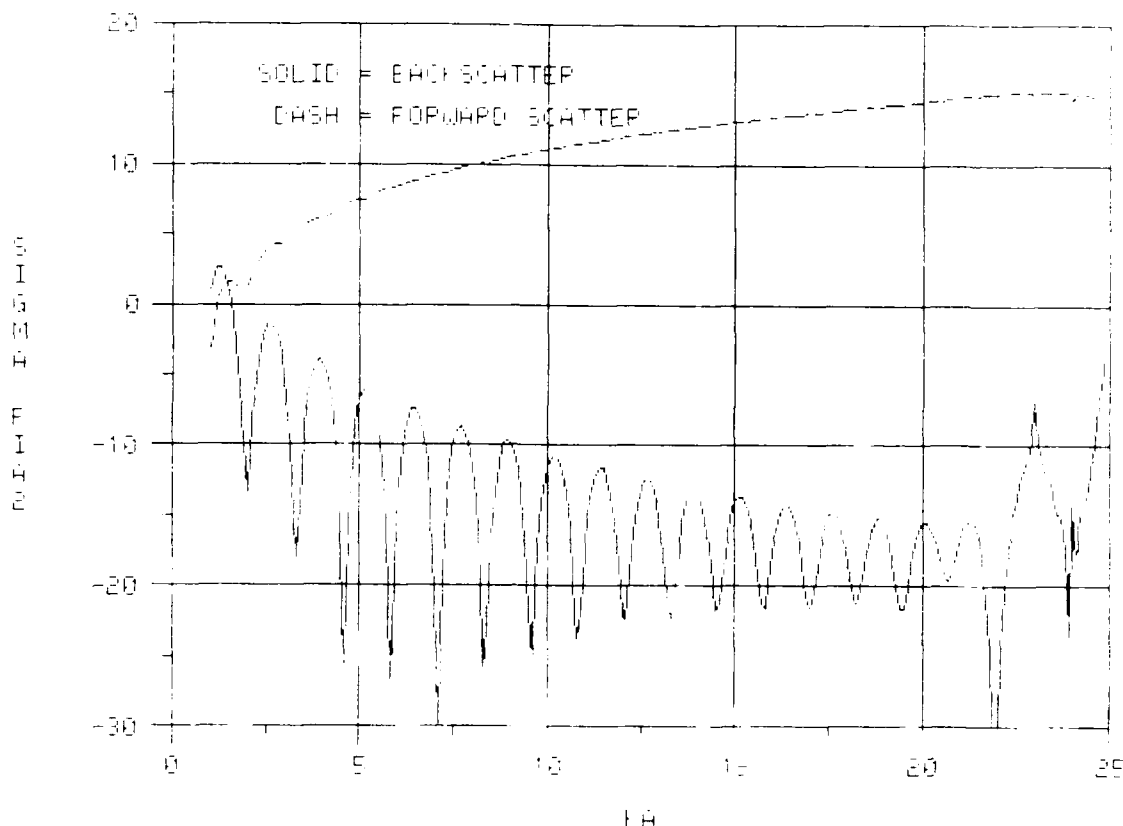


Figure 4. Grazing Incidence ka Plot

Figure 5 through Figure 8 show the bistatic radar cross-section (RCS) of a disk illuminated by a plane wave at normal incidence. The plots shown are for both horizontal and vertical polarization at several ka values. For all these cases the ϕ observation angle is zero (same as ϕ incident). For horizontal polarization ($Pol = 90$), the agreement is better than for vertical polarization ($Pol = 0$). As the disk ka increases and the observation angle exceeds 45° , the PO solution begins to break down; however, the agreement between the BSRCRCS code and the eigenfunction code remains reasonable for larger angles, especially for horizontal polarization.

BISTATIC SCATTERING FROM A DISK (CO-POL)

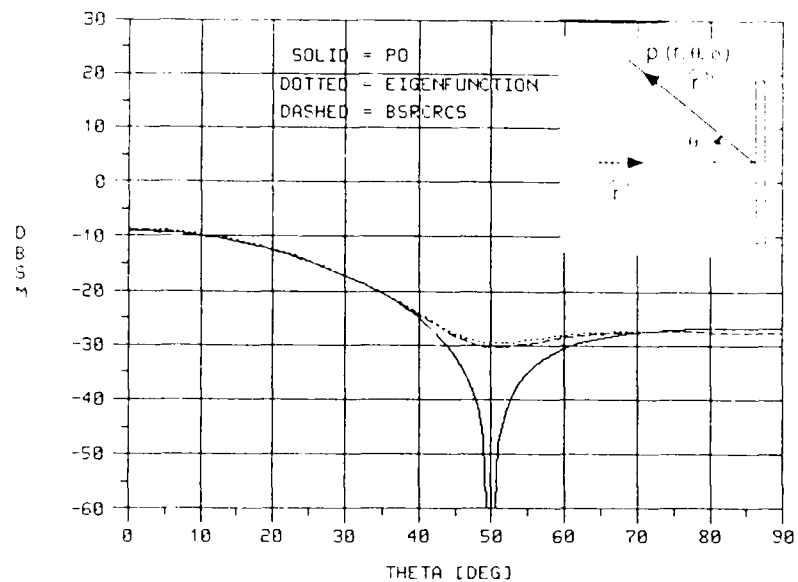


Figure 5. Bistatic Scattering: $ka = 5$: $\theta_{inc} = 0$:
 Horiz Pol: $\phi_{inc} = \phi_{scat} = 0$

BISTATIC SCATTERING FROM A DISK (CO-POL)

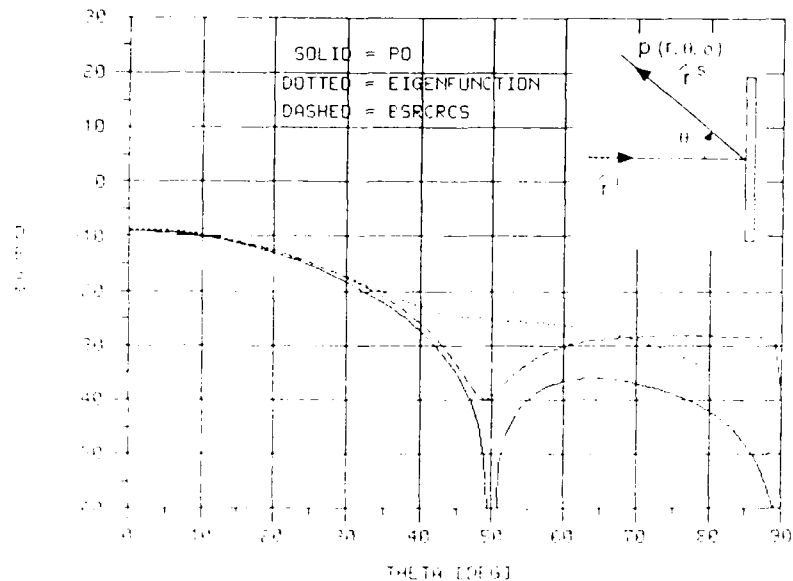


Figure 6. Bistatic Scattering: $ka = 5$: $\theta_{inc} = 0$:
 Vert Pol: $\phi_{inc} = \phi_{scat} = 0$

BISTATIC SCATTERING FROM A DISK (CO-POL)

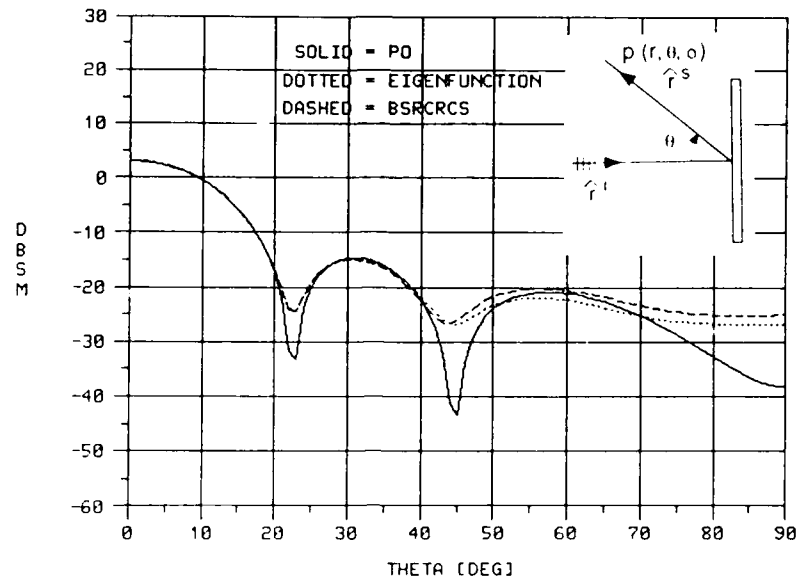


Figure 7. Bistatic Scattering: $ka = 10$: Theta Inc = 0:
Horiz Pol: Phi Inc = Phi Scat = 0

BISTATIC SCATTERING FROM A DISK (CO-POL)

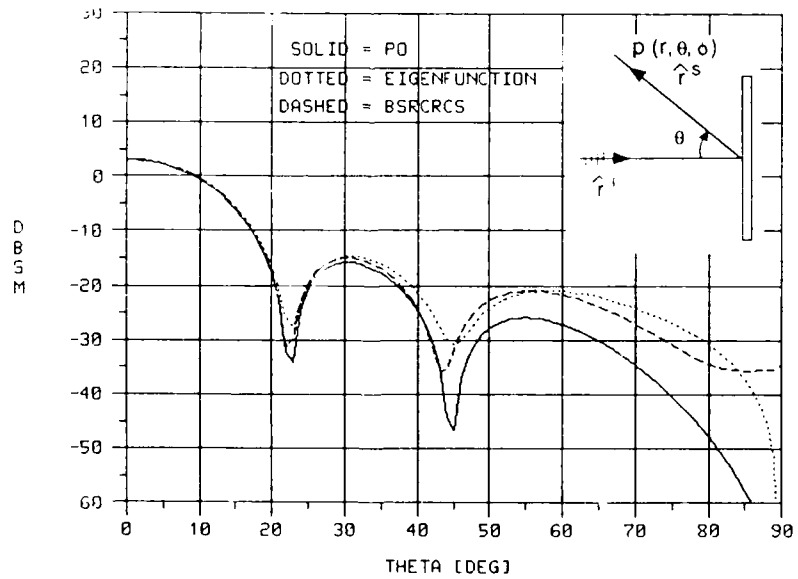


Figure 8. Bistatic Scattering: $ka = 10$: Theta Inc = 0:
Vert Pol: Phi Inc = Phi Scat = 0

Letting $\phi^S = 180^\circ$, we are in the quadrant where the specular lies for our given plane of incidence. We see that regardless of how different the results are in general, they agree (within a few dB) at specular. Figures 9 through 14 show these results for several incident angles. The agreement at specular gives us hope the calibration curve will agree over a wide range of bistatic angles.

Plotting the calibration curve, we see that the calibration curve calculated using PO goes to zero for both polarizations; however, the calibration curve calculated using the eigenfunction, as expected, does not. We see reasonable agreement for both polarizations over bistatic angles less than 140 degrees. Figure 15 through Figure 20 shows this comparison for several ka values. As ka increases, the agreement between the PO and eigenfunction solutions for specular improves. As we see in Figure 20, $ka = 20$ the difference is negligible for $0 \leq \beta \leq 140^\circ$.

4. CONCLUSIONS

Our eigenfunction code is only accurate up to $ka = 20$. Beyond that it is no longer useful.

We saw that the PO solution for normal incidence agreed very well with the eigenfunction and BSRCRCS codes over the main lobe and a significant number of side lobes. For small ka the agreement is remarkable.

When we concentrate on the specular return from the disk, PO does a good job for incidence angles as large as 70 degrees. This is really not that surprising since the specular return is an optics quantity governed by geometrical optics. In fact, the stationary phase evaluation of the PO integral gives, in general, the GO reflected field. As we saw in the calibration curves (specular response), the PO and eigenfunction solutions agree very well for large ka ; however, for small ka we would need a correction factor to use the PO curve for calibration. We saw that the disk calibration curves are well behaved and have no rapid fluctuations and there are several available methods to calculate the curve. This makes the disk an ideal candidate as a standard for bistatic RCS measurements. We also saw that the PO and eigenfunction solutions generate the same curve over a wide range of bistatic angles ($0 < \beta < 140^\circ$) for large ka . This means there exists an easy method of generating the applicable calibration curve for a particular disk as long as one remains within the valid angular region with an appropriately sized disk.

BISTATIC SCATTERING FROM A DISK (CO-POL)

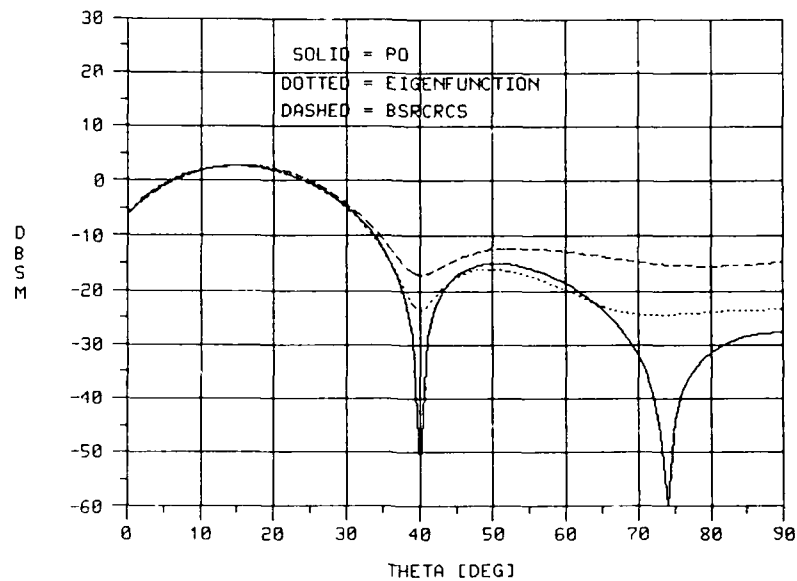


Figure 9. Bistatic Scattering: $ka = 10$: Theta Inc = 15: Horiz Pol: Phi Inc = 0: Phi Scat = 180

BISTATIC SCATTERING FROM A DISK (CO-POL)

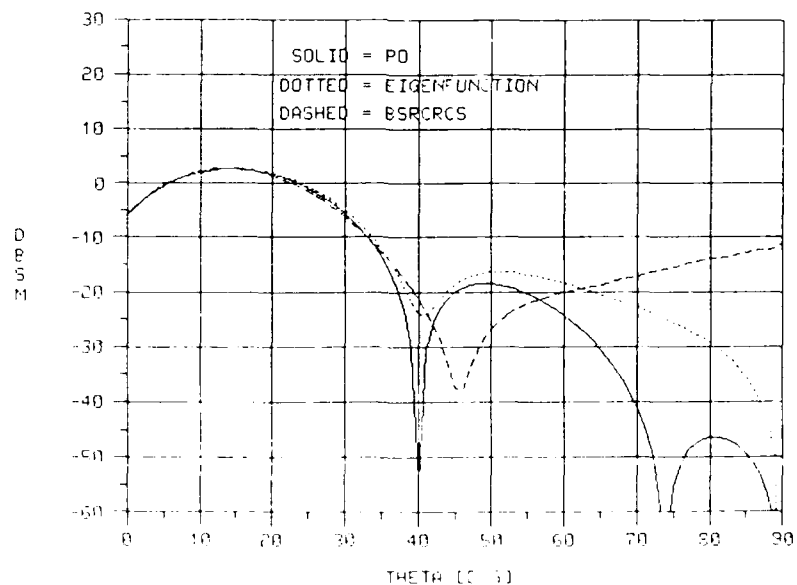


Figure 10. Bistatic Scattering: $ka = 10$: Theta Inc = 15: Vert Pol: Phi Inc = 0: Phi Scat = 180

BISTATIC SCATTERING FROM A DISK (CO-POL)

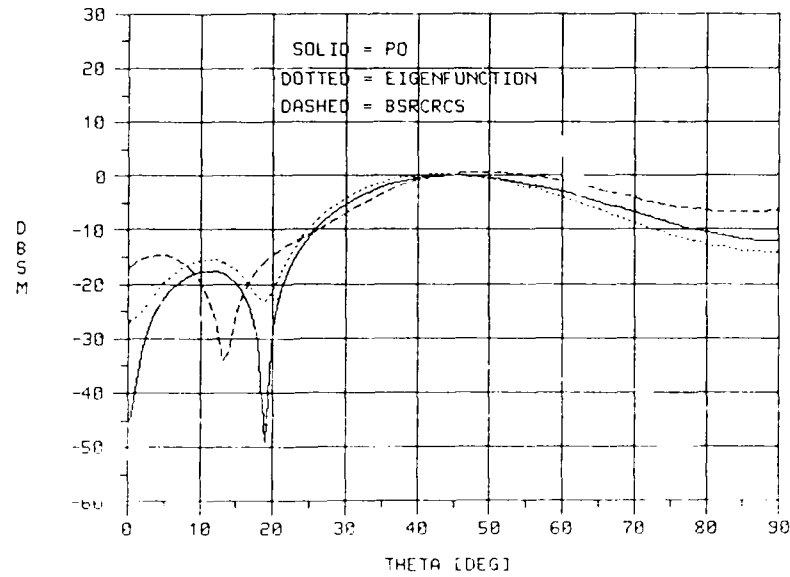


Figure 11. Bistatic Scattering: $ka = 10$: Theta Inc = 45:
Horiz Pol: Phi Inc = 0: Phi Scat = 180

BISTATIC SCATTERING FROM A DISK (CO-POL)

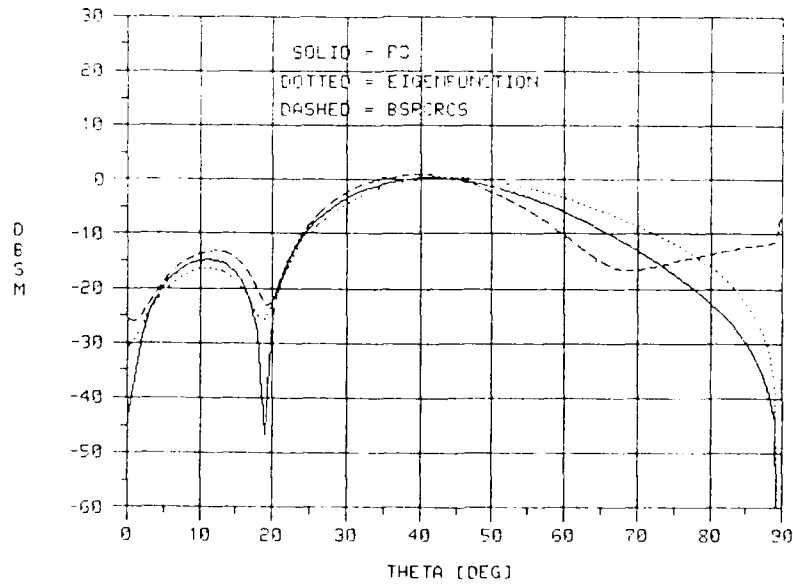


Figure 12. Bistatic Scattering: $ka = 10$: Theta Inc = 45:
Vert Pol: Phi Inc = 0: Phi Scat = 180

BISTATIC SCATTERING FROM A DISK (CO-POL)

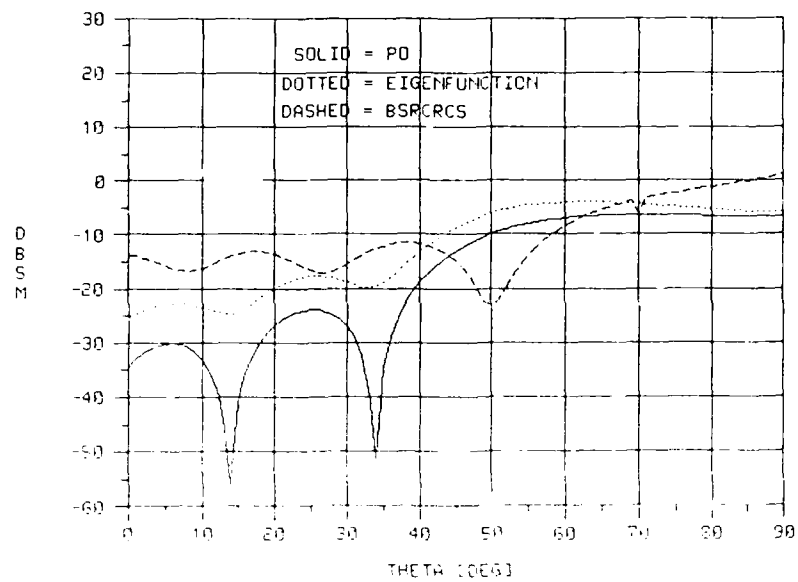


Figure 13. Bistatic Scattering: $ka = 10$: Theta Inc = 70:
 Horiz Pol: Phi Inc = 0: Phi Scat = 180

BISTATIC SCATTERING FROM A DISK (CO-POL)

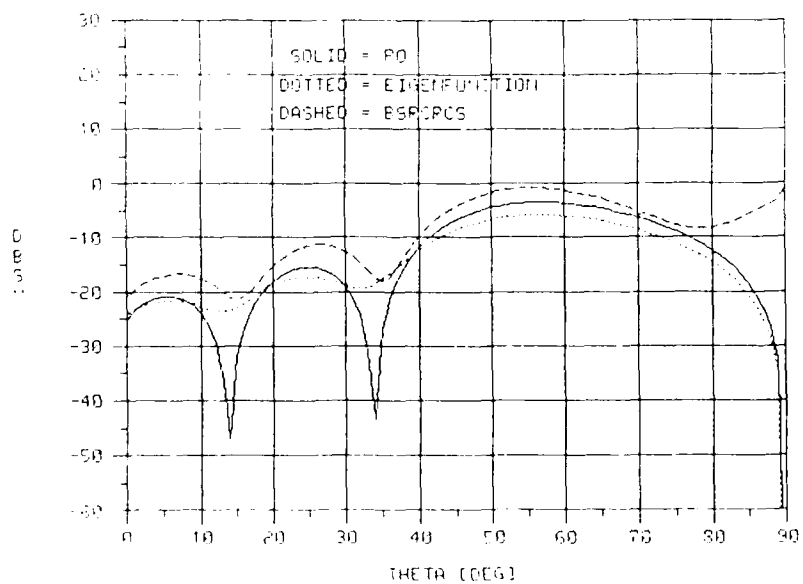


Figure 14. Bistatic Scattering: $ka = 10$: Theta Inc = 70:
 Vert Pol: Phi Inc = 0: Phi Scat = 180

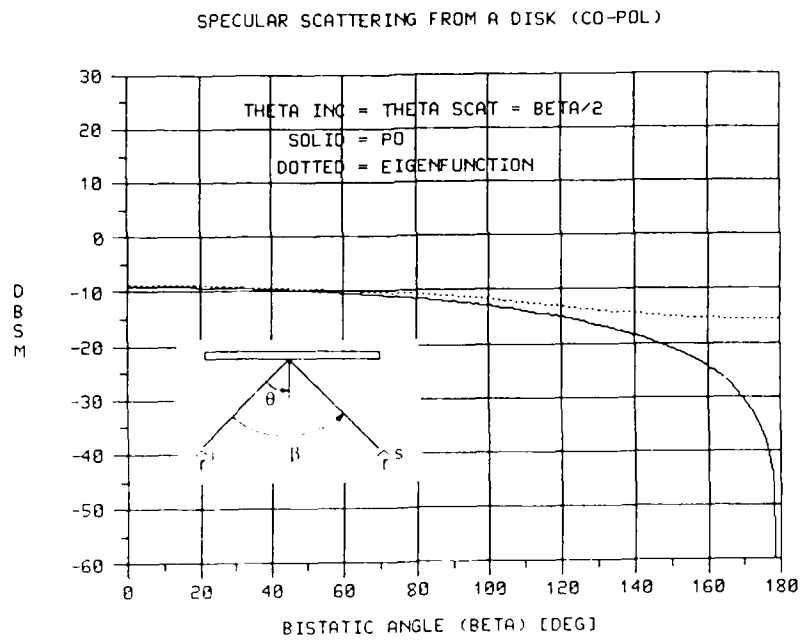


Figure 15. Specular Scattering: $ka = 5$: Horiz Pol

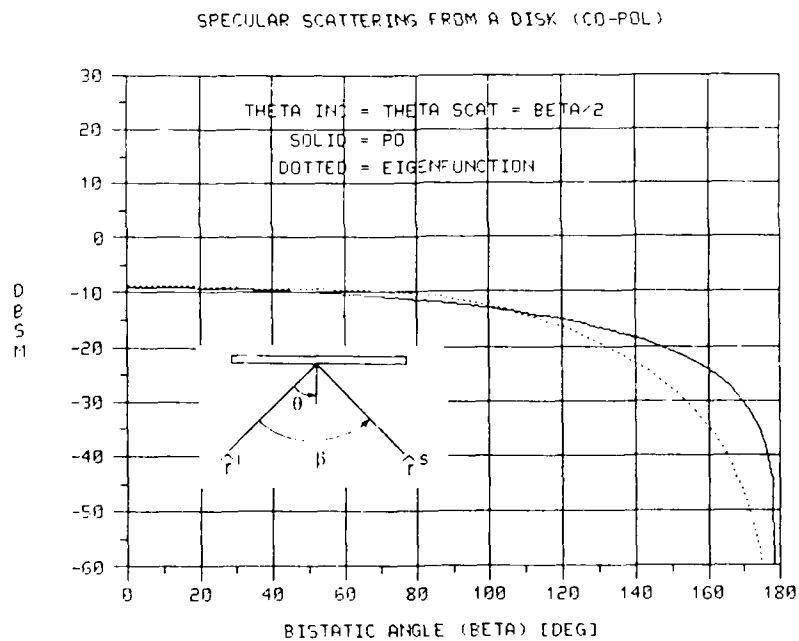


Figure 16. Specular Scattering: $ka = 5$: Vert Pol

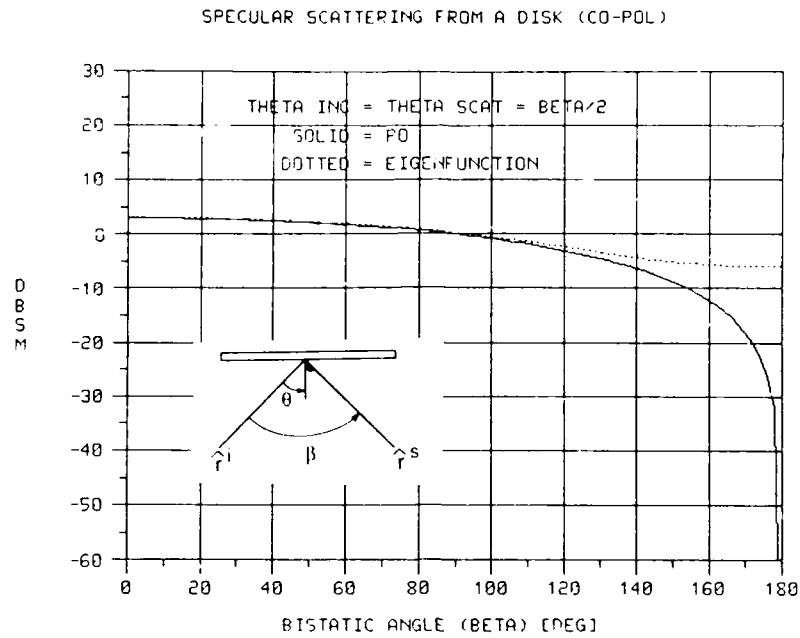


Figure 17: Specular Scattering: $ka = 10$: Horiz Pol

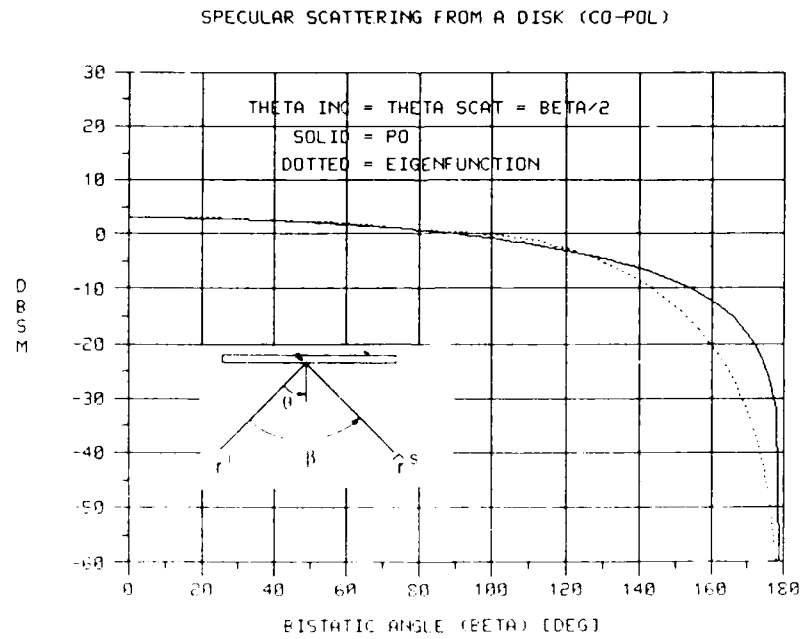


Figure 18. Specular Scattering: $ka = 10$: Vert Pol

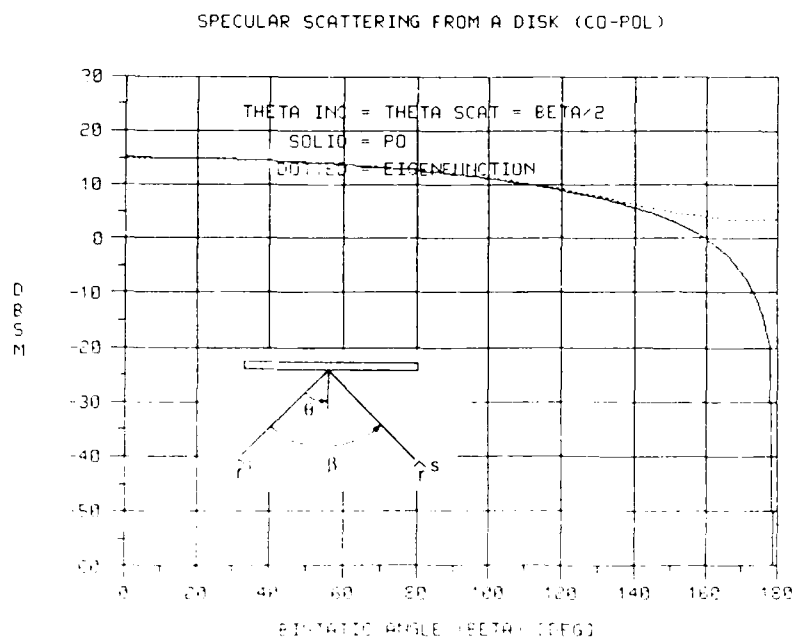


Figure 19: Specular Scattering: $ka = 20$: Horiz Pol

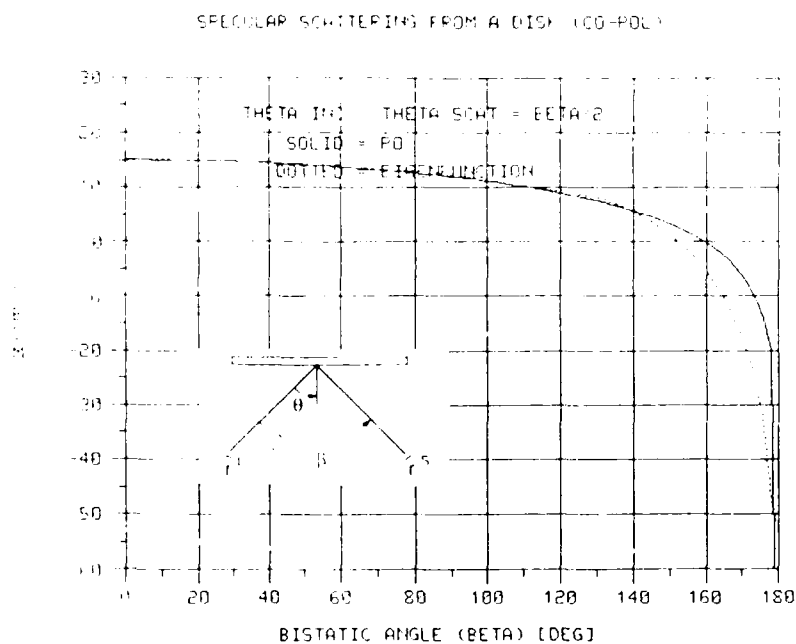


Figure 20. Specular Scattering: $ka = 20$: Vert Pol

References

1. Bowman, J. J., Senior, T. B. A., and Uslenghi, P. L. E. (Eds.) (1969) Electromagnetic and Acoustic Scattering by Simple Shapes, Chapters 13 and 14; North Holland Pub. Co., Amsterdam.
2. Flammer, C. (1953) The vector wave function solution of the diffraction of electromagnetic waves by circular disks and apertures, I. Oblate spheroidal vector wave functions, II. The diffraction problem, J. Appl. Phys., 24(No. 9):1218-1231.
3. Mattson, G. R. (1970) Electromagnetic Plane Wave Scattering by a Perfectly Conducting Disk, Ph.D. Dissertation, University of Michigan.
4. Mithouard, D. P., and Hodge, D. B. (1979) Scattering by Metallic Disk, Report 710816-3, The Ohio State University Electroscience Laboratory, Dept. of Electrical Engineering.
5. Ufimtsev, P. Ya. (1958) Approximate calculation of the diffraction of a plane electromagnetic wave by certain metal objects, II. The diffraction by a disk and by a finite cylinder, Soviet Physics - Technical Physics, 3(No. 11):2386-2396.
6. Dominek, A.K. personal communication.



MISSION of Rome Air Development Center

RADC plans and executes research, development, test and selected acquisition programs in support of Command, Control, Communications and Intelligence (C³I) activities. Technical and engineering support within areas of competence is provided to ESD Program Offices (POs) and other ESD elements to perform effective acquisition of C³I systems. The areas of technical competence include communications, command and control, battle management, information processing, surveillance sensors, intelligence data collection and handling, solid state sciences, electromagnetics, and propagation, and electronic, maintainability, and compatibility.

ATE
LMED
8